AGU100 ADVANCING EARTH AND SPACE SCIENCE

Geophysical Research Letters

RESEARCH LETTER
10.1029/2019GL082789

Key Points:
- The magnetospheric driver of STEVE is investigated using clear conjunction observations when Van Allen Probes directly crossed STEVE
- STEVE corresponds to a sharp plasmapause with SAID electric field, parallel electron acceleration collocated with kinetic Alfvén waves
- Multiwavelength continuous STEVE emissions are likely powered by parallel electron precipitation superimposed on heat conduction

Supporting Information:
- Supporting Information S1
- Movie S1
- Movie S2

Correspondence to:
X. Chu,
chuxiangning@gmail.com

Citation:
Chu, X., Malaspina, D., Gallardo-Lacourt, B., Liang, J., Andersson, L., Ma, Q., et al (2019). Identifying STEVE's Magnetospheric Driver Using Conjugate Observations in the Magnetosphere and on the Ground. *Geophysical Research Letters*, *46*, 12,665–12,674. https://doi.org/10.1029/2019GL082789

Received 11 MAR 2019
Accepted 6 NOV 2019
Accepted article online 11 NOV 2019
Published online 21 NOV 2019

Identifying STEVE's Magnetospheric Driver Using Conjugate Observations in the Magnetosphere and on the Ground

Xiangning Chu[1], David Malaspina[1], Bea Gallardo-Lacourt[2], Jun Liang[2], Laila Andersson[1], Qianli Ma[3], Anton Artemyev[4], Jiang Liu[3], Robert E. Ergun[1], Scott Thaller[1], Hassanali Akbari[1], Hong Zhao[1], Brian Larsen[5], Geoffrey Reeves[5], John Wygant[6], Aaron Breneman[6], Sheng Tian[6], Martin Connors[7], Eric Donovan[2], William Archer[8], and Elizabeth A. MacDonald[9]

[1]Laboratory for Atmospheric and Space Physics, University of Colorado Boulder, Boulder, CO, USA, [2]Department of Physics and Astronomy, University of Calgary, Calgary, Alberta, Canada, [3]Department of Atmospheric and Oceanic Sciences, University of California, Los Angeles, CA, USA, [4]Institute of Geophysics and Planetary Physics, University of California, Los Angeles, CA, USA, [5]Los Alamos National Laboratory, Los Alamos, NM, USA, [6]Department of Physics, University of Minnesota, Twin Cities, Minneapolis, MN, USA, [7]Athabasca University Observatories, Athabasca, Alberta, Canada, [8]Department of Physics and Engineering Physics, University of Saskatchewan, Saskatoon, Saskatchewan, Canada, [9]NASA Goddard Space Flight Center, Greenbelt, MD, USA

Abstract The magnetospheric driver of strong thermal emission velocity enhancement (STEVE) is investigated using conjugate observations when Van Allen Probes' footprint directly crossed both STEVE and stable red aurora (SAR) arc. In the ionosphere, STEVE is associated with subauroral ion drift features, including electron temperature peak, density gradient, and westward ion flow. The SAR arc at lower latitudes corresponds to regions inside the plasmapause with isotropic plasma heating, which causes redline-only SAR emission via heat conduction. STEVE corresponds to the sharp plasmapause boundary containing quasi-static subauroral ion drift electric field and parallel-accelerated electrons by kinetic Alfvén waves. These parallel electrons could precipitate and be accelerated via auroral acceleration processes powered by Alfvén waves propagating along the magnetic field with the plasmapause as a waveguide. The electron precipitation, superimposed on the heat conduction, could explain multiwavelength continuous STEVE emission. The green picket-fence emissions are likely optical manifestations of electron precipitation associated with wave structures traveling along the plasmapause.

1. Introduction

The aurora occurs statistically within the auroral oval around the magnetic pole (between 65° and 80° in magnetic latitude [MLAT]) (Feldstein, 1963). Auroral features are caused by the dynamics of energetic particles in the Earth's magnetosphere as they precipitate into the upper atmosphere. There are many types of ionospheric photon emissions, which are generally generated by impact excitation by (1) precipitating electrons followed by the deexcitation of the neutrals releasing the photon such as aurora or (2) local ionospheric process such as stable red auroral (SAR) arc. Their electron source and energy are vastly different. There are two types of classic aurora, the diffuse and the discrete aurorae. Diffuse aurora is powered by energetic electron precipitation as electrons are scattered into the loss cone via wave-particle interactions (Ni et al., 2008; Thorne et al., 2010). Discrete aurora is caused by precipitating electrons between 1 and 10 keV accelerated by quasi-static field-aligned potential drop located several thousand km or even a few R_E above the Earth (Hull et al., 2003; Mozer et al., 1977). The electrons could also be accelerated to a few hundred eV by time-dependent Alfvén waves with strong Poynting flux (Chaston et al., 2003; Ergun et al., 2001; Keiling et al., 2003; Lysak & Song, 2003; Wygant et al., 2002). In addition to precipitation, local ionospheric processes cause emission classified as airglow (often referred as dayglow or nightglow; Solomon, 2017, and reference therein) or SAR arc by heat conduction from the magnetosphere (Barbier, 1958; Hoch & Lemaire, 1975; M. Rees & Roble, 1975; Shiokawa et al., 2013).

A distinctive emission feature, strong thermal emission velocity enhancement (STEVE), was reported by the scientific community (MacDonald et al., 2018) with the help of citizen scientists via Aurorasaurus

(MacDonald et al., 2015). It occurs in the subauroral region equatorward of the auroral oval, and it is narrow in latitude and wide in longitude. In addition, STEVE has green "picket-fence" auroral features which propagate westward along "purple" emission feature. In MacDonald et al. (2018), a STEVE event was studied using conjunction observations from the Redline Emission Geospace Observatory (REGO) all-sky imager (ASI) at Lucky Lake (LUCK) and a Low Earth Orbit Satellite Swarm-B. In the ionosphere, STEVE was accompanied by increased electron temperature, plasma density gradient, westward ion velocity, and weak magnetic perturbations indicative of field-aligned currents (FACs), which are the ionospheric features of a subauroral ion drift (SAID). A recent study, using observations from the Low Earth Orbit satellite POES-17, showed that STEVE might not be associated with >keV particle precipitation, suggesting that STEVE might be generated by local ionospheric processes (Gallardo-Lacourt, Liang, et al., 2018). However, the lowest energy channel of the particle detectors onboard POES-17 measured the total flux integrated between 50 and 1,000 eV; therefore, it cannot rule out the possibility of lower-energy ions or electrons. Mendillo et al. (2016) observed a SAR event with red and green emissions with horizontal patches, similar to STEVE, associated with the ionospheric density trough and electron temperature peak. They suggested that low-energy electron precipitation superimposed on heat conduction could explain the observations.

While this paper was under review, we became aware of an independent study (Nishimura et al., 2019) examining STEVE events using magnetospheric and ionospheric satellites. The magnetospheric spacecraft crossed a region near the edge of imagers' field of view outside of where STEVE could be identified. Several aspects of the current study are consistent with Nishimura et al. (2019) including ionospheric features of SAID (ion drift, electron heating, waves, and FAC) and magnetospheric features (nearby structured plasma boundary, flows, and waves just outside the plasmasphere). Both studies identify the importance of heat flux (or heat conduction) for "purple" STEVE emission. Nishimura et al. (2019) argued that when THEMIS ASI did not observe green picket-fence emission, no ~keV electron precipitation was present.

In this study, we examine a clear conjunction when Van Allen Probes' footprints directly crossed STEVE and a SAR arc. This conjunction provides a unique opportunity to investigate various aspects of STEVE's magnetospheric driver, including (i) STEVE maps to a sharp plasmapause boundary, (ii) identification of azimuthal ion drift at $E \times B$ drift velocity, (iii) identification of electromagnetic kinetic Alfvén waves (KAW) and corresponding low-energy parallel electron acceleration, (iv) STEVE (mapping to the plasmapause) has multiple-wavelength emissions, while the SAR arc at lower latitude mapping inside the plasmapause was redline only, and (v) this SAR arc is driven by heat conduction from isotropic electron acceleration inside the plasmapause, while low-energy precipitating electrons superimposed on heat conduction at the plasmapause are essential to generate multiwavelength STEVE emission.

2. Observations

We report a STEVE event that occurred on 17 July 2018 in conjunction with ground-based ASIs, Swarm-B satellite, and two Van Allen Probes. STEVE occurred during a 2-hr period of continuous activity, consistent with a previous study (Gallardo-Lacourt, Nishimura, et al., 2018). The Sym-H index started to decrease around 04:30 UT and reached −30 nT around 07:30 UT. The THEMIS AL index started to drop around 05:20 UT and reached a minimum of −600 nT.

2.1. Ground-Based Optical Observations

STEVE was captured by two white-light THEMIS ASIs at Athabasca and Pinawa between 06:30 UT and 07:20 UT on 17 July 2018. Figure 1 shows the long and narrow band of the continuous STEVE emission at four selected times (see supporting information Movie S1 for the entire image sequence). The continuous emission of STEVE was captured by a REGO-ASI at LUCK (the same four times in Figure S1) and Athabasca University GeoSpace Observatory (AUGSO) at Athabasca. In addition, both the continuous narrow "purple" emission and green picket-fence structures were captured by two citizen scientists, from both northern and southern sides of STEVE (photographs by Colin Chatfield and Neil Zeller are available in Figure S2). The purple and green emissions overlapped near the zenith (Figure S2b), suggesting that two emissions were aligned nearly along the magnetic field lines. The continuous emission was located higher in altitude than the green emission when viewed away from the zenith (Figure S2a). STEVE was ~0.2° wide in MLAT and a few hours wide in magnetic local time (MLT). STEVE occurred at about 61° MLAT, gradually moved equatorward to ~59.5° MLAT, and faded away afterward. In addition to STEVE, the REGO-LUCK and Athabasca

10.1029/2019GL082789

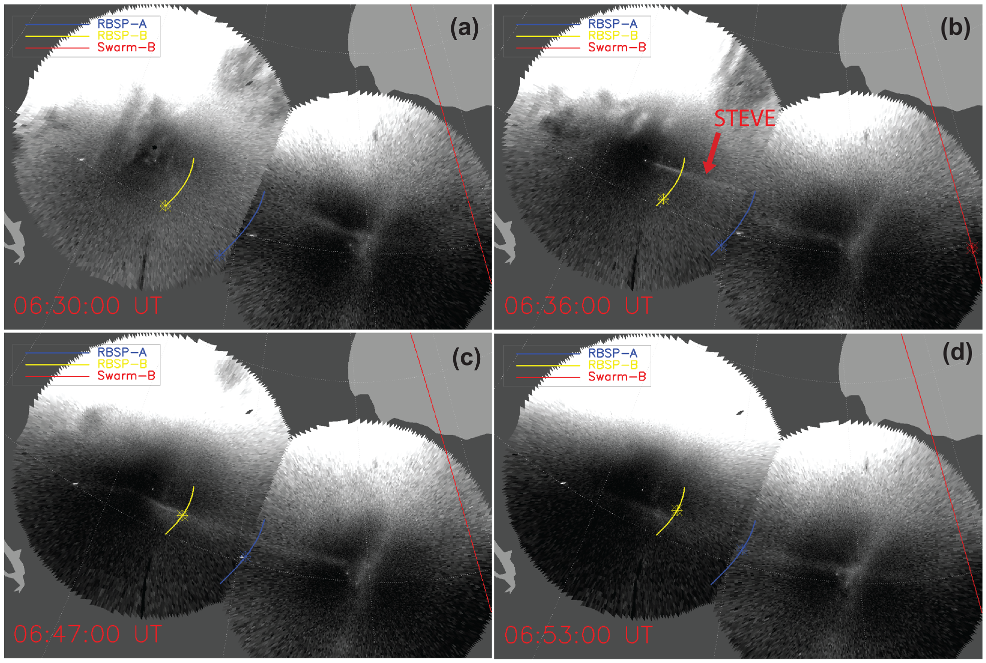

Figure 1. The STEVE event observed on 17 July 2018 by the THEMIS ASI at ATHA and PINA at (a) 06:30:00, (b) 06:36:00, (c) 06:47:00, and (d) 06:53:00 UT, with the footprints of Van Allen Probes and Swarm-B.

University GeoSpace Observatory ASIs also observed an east-west-aligned SAR arc, which was only visible in the redline emission (Mendillo et al., 2013). Different observational characteristics between STEVE and the SAR arc (Figures 1 and S1) during this event are listed below. (1) Spectrum difference. While the SAR arc was only visible in the 630.0-nm (redline) emission, STEVE was visible in multiwavelength emissions including 630.0, 557.7 nm (typical green aurora), 486.1 nm (H-beta emission), 620.0 (background for 630.0), and 480.0 (background for 486.1). This suggests that STEVE has strong redline emissions in addition to slightly enhanced emissions in various wavelengths, which is consistent with an independent study accepted during a revision of our paper (Gillies et al., 2019). (2) The SAR arc started earlier than STEVE; (3) it was thicker and was located at a lower latitude. Their differences in emission spectrum, timing, duration, and morphology suggest that STEVE and the SAR arc have different generation mechanisms. With the overlaps in the fields of view between the ASIs, the STEVE peak emission altitude was determined using traditional triangulation method to be ~280 km. This STEVE altitude corresponds to the altitude of maximum ionization rate of low-energy electrons (~100 eV) (Manfred Rees, 1964). Uncertainties of the altitude estimate could be contributed from many factors and require further investigation.

The proton aurora, equatorward of the discrete aurora, was observed by Forty-Eight Sixty-One (FESO) meridian scanning photometers that record proton aurora emission at 486.1 nm (Unick et al., 2017) at LUCK and Athabasca University. The proton aurora was located a few degrees poleward of STEVE during this event (see Figure S3). Therefore, STEVE did not correspond to the classic proton aurora or discrete electron auroral arcs (further poleward than proton aurora) (Davis, 1978; Yahnin et al., 1997), consistent with MacDonald et al. (2018).

2.2. Ionospheric Observations: Swarm

Ionospheric variations associated with STEVE were observed by Swarm-B. The Swarm constellation consists of three identical satellites (Friis-Christensen et al., 2006). Swarm-B has an altitude of ~530 km, while the other two satellites fly almost side-by-side at ~480 km. Each Swarm satellite carries high-precision and high-resolution instruments (Knudsen et al., 2017; Ritter et al., 2013) to measure magnetic field, ion flow velocity, ion and electron temperatures, and plasma density.

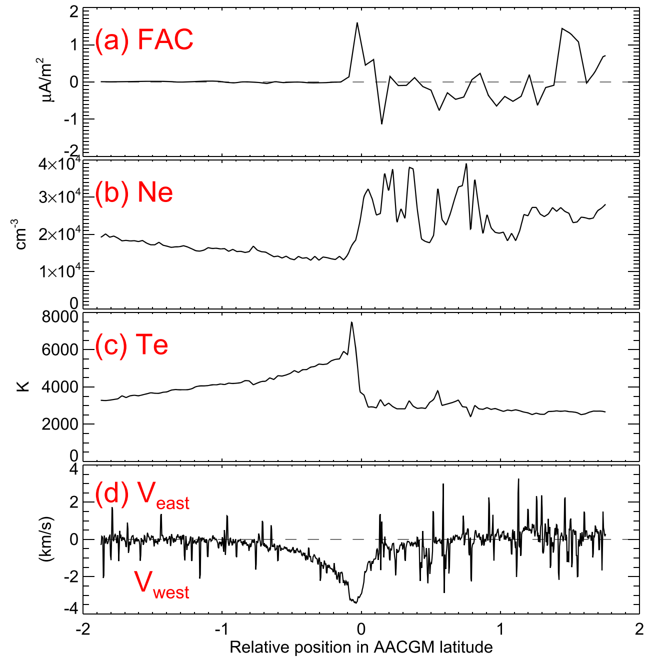

Figure 2. Ionospheric observations of STEVE versus relative latitude when Swarm-B crossed east of the STEVE (06:35:45 UT). The panels show (a) field-aligned currents, (b) electron density, (c) electron temperature, and (d) ion drift (positive eastward and negative westward).

Swarm-B crossed east of STEVE at ~06:35:45 UT (red line in Figure 1). Observed ionospheric features (Figure 2) were consistent with an SAID (MacDonald et al., 2018), which was located at the poleward edge of the subauroral region. The FACs (Figure 2a), calculated from observed magnetic perturbations, were ~1.0 μA/m^2 narrow upward (negative) at higher latitudes and ~1.0 μA/m^2 thicker downward (positive) at lower latitudes. The FACs were associated with the local current on the plasmapause (see section 2.3). The electron density (Figure 2b) showed a sharp gradient from 1.3 × 10^4 cm^{-3} at lower latitudes to 4.0 × 10^4 cm^{-3} at higher latitudes. The ion velocity (Figure 2d) showed a peak at the STEVE latitude, reaching a westward speed of 3 km/s corresponding to a strong poleward electric field. The electron temperature (Figure 2c) increased from 2,500 K outside to 7,600 K at its center, which was extremely high. Electron heating to a few thousand K is known to produce red auroral emission at 630.0 nm by exciting the lowest electronic state in atomic oxygen O(1D), which is responsible for SAR arcs (Förster et al., 1999; Foster et al., 1994; Sazykin et al., 2002). The above features are consistent with the signatures of SAID in the ionosphere (Anderson et al., 1993; Galperin, 2002; He et al., 2014; Mishin, 2013; Puhl-Quinn et al., 2007; Spiro et al., 1977).

2.3. Magnetospheric Observations: Van Allen Probes

STEVE's magnetospheric driver is investigated using the observations from the Van Allen Probes as shown in Figure 3. Van Allen Probes are two identical spacecraft in nearly the same highly elliptical, low inclination orbits (1.1 × 5.8 R_E, 10°) (Mauk et al., 2012). During this event, two Van Allen Probes traveled tailward, from the plasmasphere into the plasma sheet at premidnight local time. Their magnetic footprints crossed STEVE successively around 06:53 UT and 06:47 UT at two separated MLTs (Figure 1). As their footprints traversed STEVE (indicated by the luminosity peaks at their footprints, Van Allen Probe-B shown), they crossed the plasmapause where the plasma density (Figure 3c) decreased from ~1,000 to 10 cm^{-3} within 500 km (<0.1 R_E). The plasma density is inferred from the upper hybrid resonance frequency observed by the EMFISIS instrument (Kurth et al., 2015). In addition, their footprints crossed the SAR arc inside the plasmapause at lower latitudes (Figure 3b).

STEVE is associated with an SAID at the plasmapause. The background magnetic field was mainly northward in GSM coordinates with an amplitude of ~270 nT. The magnetic perturbations (Figure 3d,

10.1029/2019GL082789

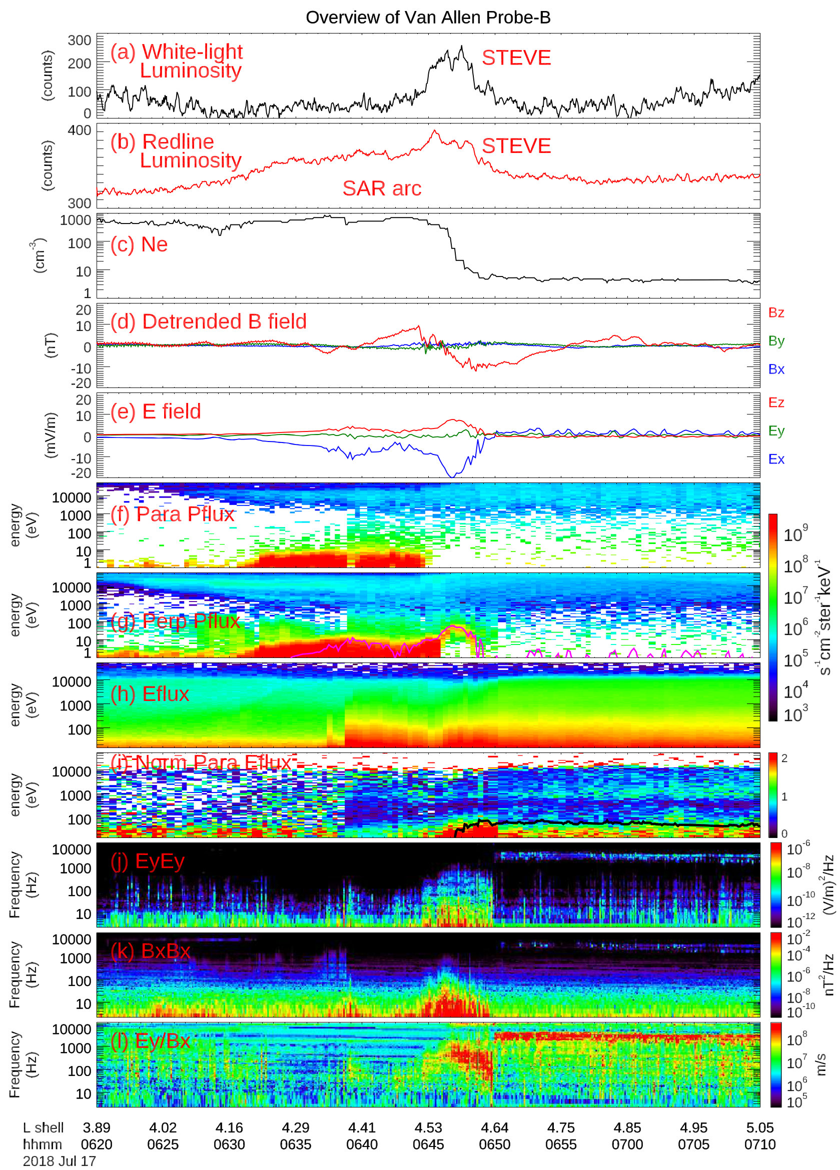

Figure 3. Overview of magnetospheric observations. (a) Auroral luminosities at the footprints from white-light ASIs; (b) redline auroral luminosities at the footprints; (c) electron density; (d) detrended magnetic fields in GSM coordinates; (e) electric field vectors in mGSE coordinates; (f) parallel differential proton flux at PA = 18°; (g) perpendicular differential proton flux at PA = 90°; the purple line represents the proton energy ($1/2m_pV_{E\times B}^2$) at the speed of $V_{E\times B}$ drift; (h) omnidirectional electron flux; (i) normalized parallel differential electron flux at PA = 18°; the black line represent the electron energy accelerated by the KAW; (j and k) power spectra of the electric field (E_{YFAC}) and the magnetic field (B_{XFAC}) in FAC coordinates; (l) the ratio of E_{YFAC}/B_{XFAC}.

subtracted by the IGRF model and detrended with a 20-min window) showed a bipolar pattern in the northward component (Bz) with a peak-to-peak variation of ~20 nT at the plasmapause suggesting the existence of local current. A strong tailward quasi-static electric field of approximately −20 mV/m (Figure 3e) was observed at the plasmapause by Van Allen Probe-B (the DC-coupled electric field and other measurements on Van Allen Probe-A were similar and not shown because they were not reliable during this event due to radiation damage accumulated by the preamplifiers). This strong electric field corresponded to a strong westward plasma drift velocity $V_{E\times B}$ of ~80 km/s. The strong and narrow electric field is a typical feature of an SAID in the equatorial magnetosphere (Mishin, 2013, and references therein). The observed SAID coincided with the inner edge of the ion plasma sheet, which is similar to subauroral polarization streams (Foster & Vo, 2002; Southwood & Wolf, 1978; Yeh et al., 1991). This local current and the ionospheric FACs were likely caused by the misalignment of gradient in the ring current pressure (see last discussion paragraph) and magnetic flux volume (Vasyliunas, 1970; Wolf, 1983, 1995). The FACs flow into regions of low ionospheric conductivity (low ionospheric electron density observed by Swarm-B), which lead to the observed large electric field in order to maintain current continuity (Foster & Burke, 2002).

In this event, the ion and electron energies near the plasmapause reached a few hundred V as observed by the HOPE instrument (Funsten et al., 2013) simultaneously with the strong quasi-static electric field. The spacecraft floating potential of Van Allen Probe-B was only a few V, suggesting that the observed plasma energy was real. The proton energy increased from a few eV to a few hundred eV at the peak of the electric field and then dropped back. These protons were mostly perpendicular to the magnetic field, since the perpendicular proton flux was much higher than the parallel flux. The purple line in Figure 3g, which is the energy of protons moving at the speed of $V_{E\times B}$ drift ($1/2m_pV_{E\times B}2$), agrees well with the observed proton flux peak energy. This fact suggests that the protons were drifting at the electric field drift velocity (not stochastic heating). Since the proton drift velocity at the plasmapause was perpendicular, it is unlikely that they precipitated into the ionosphere.

The electrons at the plasmapause were accelerated to a few hundred eV. The electron acceleration, on the other hand, was stochastic and mostly in the parallel direction (Figure 3i, the ratio of the parallel electron flux to the omnidirectional flux in Figure 3h). This parallel electron acceleration was associated with strong KAW at the plasmapause (Figures 3j–3l). The electric and magnetic field wave power spectra from EMFISIS were rotated into local field-aligned coordinates. Z_{FAC} is along the magnetic field B, Y_{FAC} is perpendicular to both the spin axis and B (roughly westward), and X_{FAC} completes the orthogonal set (roughly sunward). The power spectra in E_{YFAC} and B_{XFAC} (Figures 3j and 3k) show strong broadband waves, and the ratio of E_{YFAC}/B_{XFAC} (Figure 3l) indicates that the Alfvén waves were Doppler-shifted by the drift velocity $V_{E\times B}$, which is a typical signature of KAW (Chaston et al., 2014). The black line in Figure 3i represents the maximum possible electron energy due to acceleration by the parallel electric field of the KAW (Artemyev et al., 2015; Kletzing, 1994). The fact that the parallel accelerated electron flux stayed below the black line suggests that the parallel electrons were accelerated by the local KAW. Note that the electron acceleration was underestimated because the integration did not include wave powers below the low-frequency cutoff of EMFISIS (4 Hz), which explains why the black line was lower coinciding with the KAW. These parallel low-energy electrons (less than a few hundred eV), if their pitch angles were within the local loss cone (7°), may precipitate into the ionosphere and contribute to the generation of STEVE. However, the pitch angle resolution of the HOPE instrument is too large (18°) to resolve the loss cone and directly calculate the energy flux of the electron precipitation. We have estimated an upper limit to the energy flux of the electron precipitation of 0.068 erg/cm^2/s when mapped to the ionosphere using the method developed by (Mozer, 1970). Yet it is too weak to generate visible aurora which requires ~1 erg/cm^2/s (Kivelson & Russell, 1995). There were substantially enhanced low-energy parallel electrons (~1–10 eV), however, which could transport heat flow into the topside ionosphere and result in electron heating during this event (Evans & Mantas, 1968; Liang et al., 2017; Moffett et al., 1998; M. Rees & Roble, 1975; Slater et al., 1987). In addition, the electromagnetic energy of the KAW propagated along magnetic field lines and could accelerate the precipitating electrons through auroral acceleration processes close to the Earth (Chaston et al., 2003; Keiling et al., 2003; Lysak & Song, 2003; Tian, 2017; Wygant et al., 2002), which could contribute to the generation of STEVE emissions (see section 3).

Inside the plasmapause, the protons (Figures 3f and 3g) were heated isotropically and stochastically to tens of eV in both parallel and perpendicular directions. The electrons flux increased to a few hundred eV, suggesting that the entire region had substantially enhanced 1- to 10-eV electrons. In addition, the protons with tens of keV plasma sheet energy were observed inside the plasmapause, and their energies decreased as they drifted across the tailward electric field region at the plasmapause, which was consistent with a ring current pressure gradient. These plasma populations inside the plasmapause coincided with the observed SAR arc, which is consistent with previous studies that the energy source of SAR arcs was related to the energy transfer from ring current ions to plasmaspheric cold electrons and ions as a result of energy degradation through Coulomb collisions (Fok et al., 1993; Kozyra et al., 1987).

3. Discussion

In this study, the magnetospheric driver of STEVE is investigated using conjunction observations when Van Allen Probes' footprint crossed STEVE and a SAR arc in the subauroral region. Swarm-B observations showed that STEVE was associated with a narrow region of strong westward ion drift corresponding to strong poleward electric field, electron temperature peak, and a bipolar pattern of FACs, which were ionospheric signatures of an SAID. Van Allen Probes observed tailward electric fields near the plasmapause with substantially enhanced ions and electrons, and this region seems to encompass both SAR arcs and STEVE. The magnetospheric driver of STEVE was located at the sharp plasmapause, which was at the poleward/outer edge of this region. The observed narrow, strong, and quasi-static electric field corresponded to westward plasma drift, which are magnetospheric features of an SAID. The electric field coincided with strong KAW, parallel acceleration of electrons, perpendicular acceleration of ions up to a few hundred eV, and energy discontinuity of penetrating plasma sheet plasma. The protons were drifting perpendicularly, while the electron acceleration by the KAWs was stochastic and parallel. In addition to STEVE, SAR arcs were observed at slightly lower latitudes and corresponded to the regions inside the plasmapause, where isotropic low-energy plasma heating was observed. This is consistent with previous studies that the energy source of SAR arcs is related to the energy transfer from ring current ions to plasmaspheric cold electrons and ions as a result of energy degradation through Coulomb collisions (Fok et al., 1993; Kozyra et al., 1987).

The conjunction observations show that STEVE is an optical manifestation of an SAID at a sharp plasmapause. In this event, the morphological characteristics of STEVE gave clues as to its magnetospheric driver. Its occurrence at the poleward/tailward edge of the active subauroral region was consistent with the fact that its driver, an SAID, occurred at the plasmapause earthward of the plasma sheet. It was narrow in latitude and extended several hours in MLT, consistent with the fact that the SAID electric field at the plasmapause was radially narrow and azimuthally broad enough to be seen at different MLTs by two Van Allen Probes and Swarm-B. STEVE lasted about 1 hr, which was consistent with the duration of an SAID (Mishin, 2013, and references therein).

Both the strong continuous narrow “purple” emission and green picket-fence structures were captured by citizen scientists. STEVE's morphological features and different emission wavelengths suggest the presence of multiple underlying mechanisms discussed below.

The continuous STEVE emission was partly contributed by the redline emission due to the ionospheric electron heating (similar to SAR arc). Previous studies suggest that redline emission could be many kR for $T_e >$ 4,000 K (Carlson et al., 2013; Kozyra et al., 1990). During the STEVE event, the ionospheric electron temperature reached a peak of ~7,600 K. The ionospheric electron heating is usually caused by the heat conduction from the magnetosphere (Liang et al., 2017; Sazykin et al., 2002). Such a high electron temperature could contribute to the redline emission of STEVE observed by REGO at LUCK, which is estimated below. The volume emission rate at 630.0 nm as a line-of-sight integral from (Carlson et al., 2013) is

$$I_{630} = \int_{250\ \mathrm{km}}^{650\ \mathrm{km}} \alpha(Te(h))No(h)Ne(h)\mathrm{d}h, \tag{1}$$

where $\alpha(Te) = 0.15\sqrt{Te}\frac{(8537+Te)}{(34{,}191+Te)^3}\exp(-22,756/Te)$ is the O(^{1}D) thermal electron excitation rate in cm^3/s and oxygen density No(h) and electron density N_e(h) are in cm^{-3} and temperature T_e in K. N_e is the parameter of least impact on the integrated intensity of thermal 630.0-nm emission, and T_e clearly dominates (Carlson et al., 2013). Since the observations were insufficient to directly resolve the emission rate, we have compared our event with a SAR arc reported by Foster et al. (1994). A red arc with 350 R brightness corresponded to T_e of 3,500 to 4,000 K and N_e ~2.0×10^4 cm^{-3} at 450 km (slightly higher than 1.3×10^4 cm^{-3} at 530 km for our event). Since T_e is the dominating parameter, T_e ~ 7,600 K could have produced red auroral emission of 7 to 17 kR, which is visible to human eye. Note that the emission may be somewhat overestimated because the ionospheric electron density is usually more depleted within stronger ionospheric flow. Nevertheless, the redline emission during STEVE was strong due to the extreme T_e.

The multiwavelength continuous STEVE emissions could also be contributed by the equatorial parallel-accelerated electrons, which may precipitate and be accelerated by the auroral acceleration processes. Precipitating electrons into the atmosphere can be accelerated by two mechanisms: quasi-static potential

10.1029/2019GL082789

drops and time-dependent wave activity. In this study, observations at appropriate altitudes and latitude were not available to analyze if any parallel potential drop developed. The estimated energy flux of the equatorial precipitating parallel electrons was too weak to produce any visible emission. However, the precipitating electrons can be further accelerated to a few hundred eV via auroral acceleration processes powered by Alfvén waves, which propagated along the magnetic field with the plasmapause acting as a waveguide (Dmitrienko & Mazur, 1985). This is consistent with the electron energy (~100 eV) corresponding to the maximum ionization at the STEVE altitude (Mendillo et al., 2016; Manfred Rees, 1964).

The westward traveling green picket fence of STEVE was likely related to electron precipitation driven by strong waves traveling along the plasmapause. The lifetime of the green line auroral emission (<1 s) is shorter than the redline emission (~tens of s) (Gustavsson et al., 2001). Therefore, the green emission is likely an instantaneous optical manifestation of the electron precipitation produced by strong Alfvén waves, whereas the redline emission is the accumulation of the electron precipitation by these waves. Previous studies have suggested the existence of ballooning instability, shear-flow instability (Kelley, 1986; Lakhina et al., 1990), interchange stability (Sazykin et al., 2002), or Kelvin-Helmholtz instability (Lui et al., 1982) at the plasmapause associated with density gradient and/or azimuthal flows. Instabilities and waves are clearly at work at the sharp plasmapause where strong density and temperature gradients coexisted with strong azimuthal flow shear. Which instabilities are active is a challenging question and will require further investigation with more conjugate observations.

4. Conclusion

The magnetospheric driver of STEVE is investigated using conjunction observations when two Van Allen Probes directly crossed STEVE and a SAR arc in the subauroral region. In the ionosphere, STEVE was associated with an SAID, featuring with narrow westward ion drift corresponding to poleward electric field, FACs, electron temperature peak, and density gradient. In the magnetosphere, Van Allen Probes observed tailward electric fields near the plasmapause with substantially enhanced ions and electrons. The SAR arc at lower latitudes corresponded to the region inside the plasmapause with isotropic low-energy plasma heating, from which the heat conduction could generate redline emission at 630.0 nm. On the other hand, STEVE appears to be the optical manifestation of the SAID at the sharp plasmapause: a narrow quasi-static electric field coinciding with parallel-accelerated electrons by strong KAW. These parallel electrons could precipitate and be further accelerated via auroral acceleration processes powered by Alfvén waves, which propagate along the magnetic field with the plasmapause as a waveguide. These precipitating electrons, when superimposed on the heat conduction, are important in generating the multiwavelength continuous STEVE emissions. STEVE's green picket-fence emissions were likely related to higher-energy electron precipitation modulated by the Alfvén waves traveling westward along the plasmapause.

Acknowledgments
This work was supported by NASA Awards NNX17AB81G and NAS5-01072. The authors thank Robert McPherron, Jacob Bortnik, and Jinxing Li for helpful discussions. The authors thank Colin Chatfield and Neil Zeller for their STEVE photographs, Johnathan Burchill for assistance in calibrating the Swarm ion drift measurement, and Ian Schofield for AUGSO data. We acknowledge NSSDC Omniweb for geomagnetic activity indices (spdf.gsfc.nasa.gov). The authors thank the Van Allen Probes team, especially the EFW, EMFISIS, and ECT teams for their support (rbspgway.jhuapl.edu/data_instrumentationSOC). Swarm data are available online (swarm-diss.eo.esa.int). THEMIS and REGO ASIs, FESO, and AUGSO data are available online (themis.ssl.berkeley.edu website, data.phys.ucalgary.ca website, and http://autumn.athabascau.ca/publication_data/2019GL082789RRRR). Data processing was done using SPEDAS (Angelopoulos et al., 2019).

References

Anderson, P. C., Hanson, W. B., Heelis, R. A., Craven, J. D., Baker, D. N., & Frank, L. A. (1993). A proposed production-model of rapid subauroral ion drifts and their relationship to substorm evolution. *Journal of Geophysical Research*, *98*(A4), 6069–6078.

Angelopoulos, V., Cruce, P., Drozdov, A., Grimes, E. W., Hatzigeorgiu, N., King, D. A., et al. (2019). The Space Physics Environment Data Analysis System (SPEDAS). *Space Science Reviews*, *215*(1), 9. https://doi.org/10.1007/s11214-018-0576-4

Artemyev, A. V., Rankin, R., & Blanco, M. (2015). Electron trapping and acceleration by kinetic Alfvén waves in the inner magnetosphere. *Journal of Geophysical Research: Space Physics*, *120*, 10,305–10,316. https://doi.org/10.1002/2015JA021781

Barbier, D. (1958). L'activité aurorale aux basses latitudes. *Annales de Geophysique*, *14*, 334.

Carlson, H. C., Oksavik, K., & Moen, J. I. (2013). Thermally excited 630.0 nm O(^1D) emission in the cusp: A frequent high-altitude transient signature. *Journal of Geophysical Research: Space Physics*, *118*, 5842–5852. https://doi.org/10.1002/jgra.50516

Chaston, C. C., Bonnell, J. W., Carlson, C. W., McFadden, J. P., Ergun, R. E., & Strangeway, R. J. (2003). Properties of small-scale Alfvén waves and accelerated electrons from FAST. *Journal of Geophysical Research*, *108*(A4), 8003. https://doi.org/10.1029/2002JA009420

Chaston, C. C., Bonnell, J. W., Wygant, J. R., Mozer, F., Bale, S. D., Kersten, K., et al. (2014). Observations of kinetic scale field line resonances. *Geophysical Research Letters*, *41*, 209–215. https://doi.org/10.1002/2013GL058507

Davis, T. N. (1978). Observed characteristics of auroral forms. *Space Science Reviews*, *22*(1), 77–113.

Dmitrienko, I. S., & Mazur, V. A. (1985). On waveguide propagation of Alfvén waves at the plasmapause. *Planetary and Space Science*, *33*(5), 471–477. https://doi.org/10.1016/0032-0633(85)90092-3

Ergun, R. E., Su, Y. J., Andersson, L., Carlson, C. W., McFadden, J. P., Mozer, F. S., et al. (2001). Direct observation of localized parallel electric fields in a space plasma. *Physical Review Letters*, *87*(4), 045003. https://doi.org/10.1103/PhysRevLett.87.045003

Evans, J. V., & Mantas, G. P. (1968). Thermal structure of the temperate latitude ionosphere. *Journal of Atmospheric and Terrestrial Physics*, *30*(4), 563–577.

Feldstein, Y. I. (1963). Some problems concerning the morphology of auroras and magnetic disturbances at high latitudes. *Geomagnetism and Aeronomy*, *3*, 183.

Fok, M.-C., Kozyra, J. U., Nagy, A. F., Rasmussen, C. E., & Khazanov, G. V. (1993). Decay of equatorial ring current ions and associated aeronomical consequences. *Journal of Geophysical Research*, *98*(A11), 19,381–19,393.

Förster, M., Foster, J. C., Smilauer, J., Kudela, K., & Mikhailov, A. V. (1999). Simultaneous measurements from the Millstone Hill radar and the Active satellite during the SAID/SAR arc event of the March 1990 CEDAR storm. *Annales Geophysicae-Germany*, *17*(3), 389–404.

Foster, J. C., Buonsanto, M. J., Mendillo, M., Nottingham, D., Rich, F. J., & Denig, W. (1994). Coordinated stable auroral red arc observations: Relationship to plasma convection. *Journal of Geophysical Research*, *99*(A6), 11,429–11,439.

Foster, J. C., & Burke, W. J. (2002). SAPS: A new categorization for sub-auroral electric fields. *Eos, Transactions American Geophysical Union*, *83*(36), 393–394.

Foster, J. C., & Vo, H. B. (2002). Average characteristics and activity dependence of the subauroral polarization stream. *Journal of Geophysical Research*, *107*(A12), 1475. https://doi.org/10.1029/2002JA009409

Friis-Christensen, E., Lühr, H., & Hulot, G. (2006). Swarm: A constellation to study the Earth's magnetic field. *Earth, Planets and Space*, *58*(4), 351–358.

Funsten, H. O., Skoug, R. M., Guthrie, A. A., MacDonald, E. A., Baldonado, J. R., Harper, R. W., et al. (2013). Helium, Oxygen, Proton, and Electron (HOPE) mass spectrometer for the Radiation Belt Storm Probes Mission. *Space Science Reviews*, *179*(1-4), 423–484. https://doi.org/10.1007/s11214-013-9968-7

Gallardo-Lacourt, B., Liang, J., Nishimura, Y., & Donovan, E. (2018). On the origin of STEVE: Particle precipitation or ionospheric skyglow? *Geophysical Research Letters*, *45*, 7968–7973. https://doi.org/10.1029/2018GL078509

Gallardo-Lacourt, B., Nishimura, Y., Donovan, E., Gillies, D. M., Perry, G. W., Archer, W. E., et al. (2018). A statistical analysis of STEVE. *Journal of Geophysical Research: Space Physics*, *123*, 9893–9905. https://doi.org/10.1029/2018JA025368

Galperin, Y. I. (2002). Polarization jet: Characteristics and a model. *Annales Geophysicae-Germany*, *20*(3), 391–404.

Gillies, D. M., Donovan, E., Hampton, D., Liang, J., Connors, M., Nishimura, Y., et al. (2019). First observations from the TREx Spectrograph: The optical spectrum of STEVE and the picket fence phenomena. *Geophysical Research Letters*, *46*, 7207–7213. https://doi.org/10.1029/2019GL083272

Gustavsson, B., Sergienko, T., Rietveld, M. T., Honary, F., Steen, A., Brändström, B. U. E., et al. (2001). First tomographic estimate of volume distribution of HF-pump enhanced airglow emission. *Journal of Geophysical Research*, *106*(A12), 29,105–29,123. https://doi.org/10.1029/2000JA900167

He, F., Zhang, X.-X., & Chen, B. (2014). Solar cycle, seasonal, and diurnal variations of subauroral ion drifts: Statistical results. *Journal of Geophysical Research: Space Physics*, *119*, 5076–5086. https://doi.org/10.1002/2014JA019807

Hoch, R. J., & Lemaire, J. (1975). Stable auroral red arcs and their importance for the physics of the plasmapause region. *Annales de Geophysique*, *31*, 105–110.

Hull, A. J., Bonnell, J. W., Mozer, F. S., & Scudder, J. D. (2003). A statistical study of large-amplitude parallel electric fields in the upward current region of the auroral acceleration region. *Journal of Geophysical Research*, *108*(A1), 1007. https://doi.org/10.1029/2001JA007540

Keiling, A., Wygant, J. R., Cattell, C. A., Mozer, F. S., & Russell, C. T. (2003). The global morphology of wave Poynting flux: Powering the aurora. *Science*, *299*(5605), 383–386. https://doi.org/10.1126/science.1080073

Kelley, M. C. (1986). Intense sheared flow as the origin of large-scale undulations of the edge of the diffuse aurora. *Journal of Geophysical Research*, *91*(A3), 3225–3230.

Kivelson, M. G., & Russell, C. T. (1995). In M. G. Kivelson & C. T. Russell (Eds.), *Introduction to space physics* (p. 586). Cambridge, UK: Cambridge University Press.

Kletzing, C. A. (1994). Electron acceleration by kinetic Alfvén waves. *Journal of Geophysical Research*, *99*(A6), 11,095–11,103.

Knudsen, D. J., Burchill, J. K., Buchert, S. C., Eriksson, A. I., Gill, R., Wahlund, J.-E., et al. (2017). Thermal ion imagers and Langmuir probes in the Swarm electric field instruments. *Journal of Geophysical Research: Space Physics*, *122*, 2655–2673. https://doi.org/10.1002/2016JA022571

Kozyra, J. U., Shelley, E. G., Comfort, R. H., Brace, L. H., Cravens, T. E., & Nagy, A. F. (1987). The role of ring current O^+ in the formation of stable auroral red arcs. *Journal of Geophysical Research*, *92*(A7), 7487–7502.

Kozyra, J. U., Valladares, C. E., Carlson, H. C., Buonsanto, M. J., & Slater, D. W. (1990). A theoretical study of the seasonal and solar cycle variations of stable aurora red arcs. *Journal of Geophysical Research*, *95*(A8), 12,219–12,234.

Kurth, W. S., De Pascuale, S., Faden, J. B., Kletzing, C. A., Hospodarsky, G. B., Thaller, S., & Wygant, J. R. (2015). Electron densities inferred from plasma wave spectra obtained by the Waves instrument on Van Allen Probes. *Journal of Geophysical Research: Space Physics*, *120*, 904–914. https://doi.org/10.1002/2014JA020857

Lakhina, G. S., Mond, M., & Hameiri, E. (1990). Ballooning mode instability at the plasmapause. *Journal of Geophysical Research*, *95*(A4), 4007–4016.

Liang, J., Yang, B., Donovan, E., Burchill, J., & Knudsen, D. (2017). Ionospheric electron heating associated with pulsating auroras: A Swarm survey and model simulation. *Journal of Geophysical Research: Space Physics*, *122*, 8781–8807. https://doi.org/10.1002/2017JA024127

Lui, A. T. Y., Meng, C.-I., & Ismail, S. (1982). Large amplitude undulations on the equatorward boundary of the diffuse aurora. *Journal of Geophysical Research*, *87*(A4), 2385–2400.

Lysak, R. L., & Song, Y. (2003). Kinetic theory of the Alfvén wave acceleration of auroral electrons. *Journal of Geophysical Research*, *108*(A4), 8005. https://doi.org/10.1029/2002JA009406

MacDonald, E. A., Case, N. A., Clayton, J. H., Hall, M. K., Heavner, M., Lalone, N., et al. (2015). Aurorasaurus: A citizen science platform for viewing and reporting the aurora. *Space Weather*, *13*, 548–559. https://doi.org/10.1002/2015SW001214

MacDonald, E. A., Donovan, E., Nishimura, Y., Case, N. A., Gillies, D. M., Gallardo-Lacourt, B., et al. (2018). New science in plain sight: Citizen scientists lead to the discovery of optical structure in the upper atmosphere. *Science Advances*, *4*(3), eaaq0030. https://doi.org/10.1126/sciadv.aaq0030

Mauk, B., Fox, N., Kanekal, S., Kessel, R., Sibeck, D., & Ukhorskiy, A. (2012). Science objectives and rationale for the Radiation Belt Storm Probes Mission. *Space Science Reviews*, *179*, 3–27.

Mendillo, M., Baumgardner, J., Wroten, J., Martinis, C., Smith, S., Merenda, K. D., et al. (2013). Imaging magnetospheric boundaries at ionospheric heights. *Journal of Geophysical Research: Space Physics*, *118*, 7294–7305. https://doi.org/10.1002/2013JA019267

Mendillo, M., Finan, R., Baumgardner, J., Wroten, J., Martinis, C., & Casillas, M. (2016). A stable auroral red (SAR) arc with multiple emission features. *Journal of Geophysical Research: Space Physics*, *121*, 10,564–10,577. https://doi.org/10.1002/2016JA023258

Mishin, E. V. (2013). Interaction of substorm injections with the subauroral geospace: 1. Multispacecraft observations of SAID. *Journal of Geophysical Research: Space Physics*, *118*, 5782–5796. https://doi.org/10.1002/jgra.50548

Moffett, R. J., Ennis, A. E., Bailey, G. J., Heelis, R. A., & Brace, L. H. J. A. G. (1998). Electron temperatures during rapid subauroral ion drift events. *Annales Geophysicae*, *16*(4), 450–459.

Mozer, F. S. (1970). Electric field mapping in the ionosphere at the equatorial plane. *Planetary and Space Science*, *18*(2), 259–263.

Mozer, F. S., Carlson, C. W., Hudson, M. K., Torbert, R. B., Parady, B., Yatteau, J., & Kelley, M. C. (1977). Observations of paired electrostatic shocks in polar magnetosphere. *Physical Review Letters*, *38*(6), 292–295.

Ni, B., Thorne, R. M., Shprits, Y. Y., & Bortnik, J. (2008). Resonant scattering of plasma sheet electrons by whistler-mode chorus: Contribution to diffuse auroral precipitation. *Geophysical Research Letters*, *35*, L11106. https://doi.org/10.1029/2008GL034032

Nishimura, Y., Gallardo-Lacourt, B., Zou, Y., Mishin, E., Knudsen, D. J., Donovan, E. F., et al. (2019). Magnetospheric signatures of STEVE: Implications for the magnetospheric energy source and interhemispheric conjugacy. *Geophysical Research Letters*, *46*, 5637–5644. https://doi.org/10.1029/2019GL082460

Puhl-Quinn, P. A., Matsui, H., Mishin, E., Mouikis, C., Kistler, L., Khotyaintsev, Y., et al. (2007). Cluster and DMSP observations of SAID electric fields. *Journal of Geophysical Research*, *112*, A05219. https://doi.org/10.1029/2006JA012065

Rees, M. (1964). Note on the penetration of energetic electrons into the Earth's atmosphere. *Planetary and Space Science*, *12*(7), 722–725.

Rees, M., & Roble, R. G. (1975). Observations and theory of the formation of stable auroral red arcs. *Reviews of Geophysics*, *13*(1), 201–242.

Ritter, P., Lühr, H., & Rauberg, J. (2013). Determining field-aligned currents with the Swarm constellation mission. *Earth, Planets and Space*, *65*(11), 9.

Sazykin, S., Fejer, B. G., Galperin, Y. I., Zinin, L. V., Grigoriev, S. A., & Mendillo, M. (2002). Polarization jet events and excitation of weak SAR arcs. *Geophysical Research Letters*, *29*(12), 1586. https://doi.org/10.1029/2001GL014388

Shiokawa, K., Miyoshi, Y., Brandt, P. C., Evans, D. S., Frey, H. U., Goldstein, J., & Yumoto, K. (2013). Ground and satellite observations of low-latitude red auroras at the initial phase of magnetic storms. *Journal of Geophysical Research: Space Physics*, *118*, 256–270. https://doi.org/10.1029/2012JA018001

Slater, D. W., Gurgiolo, C., Kozyra, J. U., Kleckner, E. W., & Winningham, J. D. (1987). A possible energy source to power stable auroral red arcs: Precipitating electrons. *Journal of Geophysical Research*, *92*(A5), 4543–4552.

Solomon, S. C. (2017). Global modeling of thermospheric airglow in the far ultraviolet. *Journal of Geophysical Research: Space Physics*, *122*, 7834–7848. https://doi.org/10.1002/2017JA024314

Southwood, D. J., & Wolf, R. A. (1978). An assessment of the role of precipitation in magnetospheric convection. *Journal of Geophysical Research*, *83*(A11), 5227–5232.

Spiro, R. W., Heelis, R. A., & Hanson, W. B. (1977). Implications of penetration of magnetospheric convection electric-field into mid-latitude trough. *Eos Transactions American Geophysical Union*, *58*(8), 754–754.

Thorne, R. M., Ni, B., Tao, X., Horne, R. B., & Meredith, N. P. (2010). Scattering by chorus waves as the dominant cause of diffuse auroral precipitation. *Nature*, *467*(7318), 943–946. https://doi.org/10.1038/nature09467

Tian, S. (2017). The flow of Poynting flux into the terrestrial cusp and auroral zone and its role In Powering energy intensive collisionless acceleration mechanisms.

Unick, C. W., Donovan, E., Connors, M., & Jackel, B. (2017). A dedicated H-beta meridian scanning photometer for proton aurora measurement. *Journal of Geophysical Research: Space Physics*, *122*, 753–764. https://doi.org/10.1002/2016JA022630

Vasyliunas, V. (1970). Mathematical models of magnetospheric convection and its coupling to the ionosphere. In B. M. McCormac (Ed.), *Particles and fields in the magnetosphere* (pp. 60–71). Netherlands: Springer.

Wolf, R. A. (1983). *The quasi-static (slow-flow) region of the magnetosphere*. Dordrecht: Springer Netherlands.

Wolf, R. A. (1995). Magnetospheric configuration. In M. G. Kivelson & C. T. Russell (Eds.), *Introduction to space physics* (Chap. 10, 288-328). New York: Cambridge University Press.

Wygant, J. R., Keiling, A., Cattell, C. A., Lysak, R. L., Temerin, M., Mozer, F. S., et al. (2002). Evidence for kinetic Alfvén waves and parallel electron energization at 4–6 R_E altitudes in the plasma sheet boundary layer. *Journal of Geophysical Research*, *107*(A8), 1201. https://doi.org/10.1029/2001JA900113

Yahnin, A. G., Sergeev, V. A., Gvozdevsky, B. B., & Vennerstrøm, S. (1997). Magnetospheric source region of discrete auroras inferred from their relationship with isotropy boundaries of energetic particles. *Annales de Geophysique*, *15*(8), 943–958.

Yeh, H. C., Foster, J. C., Rich, F. J., & Swider, W. (1991). Storm time electric field penetration observed at mid-latitude. *Journal of Geophysical Research*, *96*(A4), 5707–5721.